Singh et al. Nanoscale Research Letters (2017) 12:298
DOI 10.1186/s11671-017-2039-3

Nanoscale Research Letters

NANO COMMENTARY

Open Access

Shape and Size-Dependent Magnetic Properties of Fe_3O_4 Nanoparticles Synthesized Using Piperidine

Ashwani Kumar Singh[1], O. N. Srivastava[2] and Kedar Singh[1,2*]

Abstract

In this article, we proposed a facile one-step synthesis of Fe_3O_4 nanoparticles of different shapes and sizes by co-precipitation of $FeCl_2$ with piperidine. A careful investigation of TEM micrographs shows that the shape and size of nanoparticles can be tuned by varying the molarity of piperidine. XRD patterns match the standard phase of the spinal structure of Fe_3O_4 which confirms the formation of Fe_3O_4 nanoparticles. Transmission electron microscopy reveals that molar concentration of $FeCl_2$ solution plays a significant role in determining the shape and size of Fe_3O_4 nanoparticles. Changes in the shape and sizes of Fe_3O_4 nanoparticles which are influenced by the molar concentration of $FeCl_2$ can easily be explained with the help of surface free energy minimization principle. Further, to study the magnetic behavior of synthesized Fe_3O_4 nanoparticles, magnetization vs. magnetic field (M-H) and magnetization vs. temperature (M-T) measurements were carried out by using Physical Property Measurement System (PPMS). These results show systematic changes in various magnetic parameters like remanent magnetization (Mr), saturation magnetization (Ms), coercivity (Hc), and blocking temperature (T_B) with shapes and sizes of Fe_3O_4. These variations of magnetic properties of different shaped Fe_3O_4 nanoparticles can be explained with surface effect and finite size effect.

Background

Nano-sized materials on account of their surface and quantum size effect not only are known to possess better physical and chemical properties but also have enhanced biocompatibility and bioefficacy [1, 2]. In this context, magnetic nanoparticles for their unique magnetic behavior have gained much attention in recent years, whereby they are known to have promising potential for various medical applications such as targeted drug delivery systems, MRI, diagnostics, radiofrequency hyperthermia, and cancer therapy [3–7]. Besides, magnetic nanoparticles are also being utilized as a key material for magnetic ferrofluid [8], catalysis [9], data storage [10], and environmental remediation [11]. Fe_3O_4, a magnetic nanoparticle, has the cubic inverse spinal structure (two Fe^{3+} with one Fe^{2+}) in which oxygen forms an fcc closed-pack structure [12]. It is an important class of half-metallic materials, as electrons hop between Fe^{2+} and Fe^{3+}. However, their utilization for practical application still requires rectification of several parameters, broadly categorized into two main class: (a) their tendency to get aggregate in order to reduce their surface energy and (b) their ability to get oxidize easily. The aforementioned parameters can hamper their interfacial area, thereby hindering their magnetism and dispersibility. Henceforth, it becomes essentially important to overcome such parameters which possibly can be achieved by developing potential synthesis methods which overrule such problems. With the advent of several wet chemical methods for the synthesis of nanoparticles in the recent past, the magnetic nanoparticles have been synthesized by different methods such as solvothermal [13], sol-gel [14], co-precipitation [15], thermal decomposition [16], and sonochemical reaction [17]. Here in this work, we have designed a new and facile one-step synthesis of Fe_3O_4 nanoparticles by using a new chemical piperidine ($C_5H_{11}N$) by hydrolysis method. Amongst several chemicals such as ether (CH_3OCH_3) and formaldehyde (HCHO), piperidine was found most effective for the synthesis of Fe_3O_4 nanoparticles.

* Correspondence: kedarbhu08@gmail.com
[1]School of Physical Sciences, Jawaharlal Nehru University, New Delhi 110067, India
[2]Department of Physics, Banaras Hindu University, Varanasi 221005, India

Experimental

Chemicals: $FeCl_2 \cdot 4H_2O$ (anhydrous) was procured from Sigma-Aldrich, while piperidine (C_6H_5N) was procured from Merck. All chemicals were used as received. Double-distilled water was used in reaction as a medium.

Preparation of Fe_3O_4 Nanoparticles

Synthesis of Fe_3O_4 nanoparticles was made in four different sets (by varying the molarity of $FeCl_2$ solution) to study the influence of the reaction parameters on the size and shape of Fe_3O_4 nanoparticles. A solution of piperidine (50 ml, 0.25 M) was prepared by mixing 1.24 ml piperidine ($C_5H_{11}N$) homogeneously into 50 ml double-distilled water. This was used as stock solution throughout the experiments. The solutions of $FeCl_2$ (10 ml) with varying molarity (0.025, 0.05, 0.075, and 0.1 M) was prepared by dissolving 0.0497, 0.0994, 0.1491, and 0.1988 g $FeCl_2$ in double-distilled water, respectively. These samples were designated as S_1, S_2, S_3, and S_4, respectively. Now, 5 ml of prepared piperidine solution was mixed with $FeCl_2$ solution of different molarities as in above, under stirring. An instant change in color indicated the formation of Fe_3O_4 nanoparticles. The reaction mixture was then centrifuged at 10,000 rpm for 10 min. Particles were collected and resuspended in 5 ml double-distilled water for further characterizations.

Characterization

The XRD analyses of resulting samples were carried out with an X-Pert Pro X-ray diffractometer (PAN analyst BV the Netherlands with a build in graphite monochromator meter) with Cu Kα radiation ($\lambda = 1.54056$ A°). Sample preparation for XRD was done by placing one drop of the reaction mixture on a circular disk (5 mm diameter) and allowing it to dry. Transmission electron microscopic (TEM) studies were done by employing TECHNI 20 G^2 microscope at an accelerating voltage 200 KeV. Samples for TEM were prepared by suspending powder in double-distilled water and ultrasonicated it for 1 h. The suspension obtained was placed on a formvar-coated Cu grid. Magnetic measurements were performed on 14 T Physical Properties Measurement System, Cryogenics Limited, USA.

Discussion

Structural and microstructural characterization of the samples were investigated by using XRD pattern. Figure 1 represents the XRD profile of Fe_3O_4 nanoparticles synthesized with different concentrations of $FeCl_2$ solution.

The XRD pattern can be matched to the series of Bragg reflections corresponding to the standard phase of the spinal structure of Fe_3O_4 with a lattice constant of $a = 8.41$A° (ICSD82-1533). Six peaks at 30.16°, 35.49°, 43.01°, 53.78°, 57.21°, and 62.73° can be indexed as (220), (311), (400), (422), (511), and (440) of the cubic structure (Fd3m space group) of Fe_3O_4 nanoparticles.

Intensive TEM analysis was performed to investigate the shape and size of the as-synthesized Fe_3O_4 particles using piperidine. Figure 2 (S_1–S_4) depicts the typical TEM micrographs of Fe_3O_4 particles synthesized with varying molarity of $FeCl_2$ (0.025, 0.05, 0.075, and 0.1 M) with respect to piperidine. Figure 2 (S_1) depicts the TEM micrograph of the synthesized Fe_3O_4 particles synthesized with a least molar concentration of $FeCl_2$ (0.025 M). As it can be seen from Fig. 2 (S_1), particles

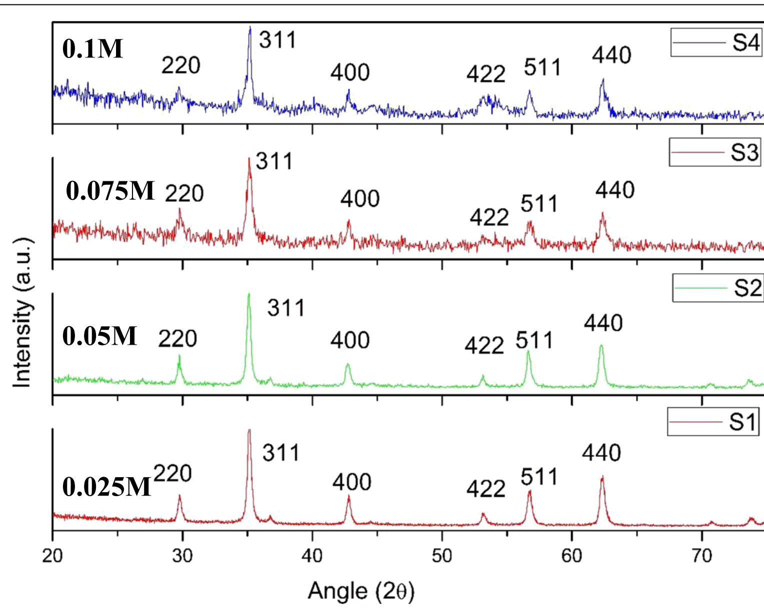

Fig. 1 The XRD profile of Fe_3O_4 nanoparticles synthesized with different concentrations of $FeCl_2$ solution

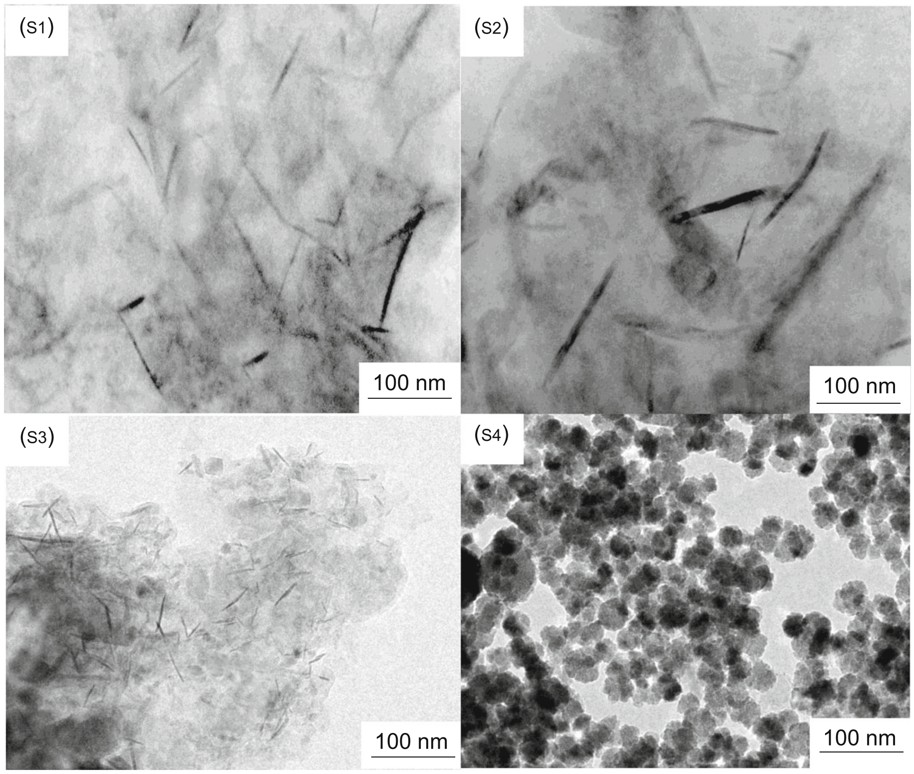

Fig. 2 TEM micrographs of as-synthesized Fe_3O_4 with varying molarity of $FeCl_2$. Notice the change in morphology with varying molarity

are nearly rod-shaped with high aspect ratio (~10) and having a length between 150 and 200 nm. As it is clearly visible that rods are tapered at the ends and maximum at the center, making it a needle-like structure, from Fig. 2 (S_2–S_4), it can be seen that with increasing molarity of $FeCl_2$ solution, aspect ratio of rod-like nanostructures decreases. At the highest molarity of $FeCl_2$ solution (0.1 M), Fe_3O_4 nanoparticles become spherical in morphology. As we know that rate of reaction plays a dominant role in the shape and size of nanocrystals, during the process of formation of nanocrystals, the growth rate is different for different crystallographic planes which are based on surface free energy minimization principle. Further, the ratio of the growth rate of different directions determines the shape of the crystal [18]. Based on the above theory, the facets with higher energy grow faster and tend to disappear, which leads to the crystal to bind by low-energy facets. This results in different morphologies of Fe_3O_4 crystals. In solution phase synthesis, it is well known that capping agents can change the free energy of different facets through their interaction with crystal surface [19, 20]. In our synthesis protocol, piperidine is used which acts as both reductant and surfactant. During the reaction of $FeCl_2$ with piperidine, somewhere in intermediate stage $Fe(OH)_2$ is formed. As the molar concentration of $FeCl_2$ is in increasing order from S1 (0.025 M) to S4 (0.1 M), formation of $Fe(OH)_2$ complex sharply increases with increasing concentration of $FeCl_2$. This fast formation rate consequence in merging the nucleation and growth steps. A separate nucleation and growth steps are a major factor for the high-quality anisotropic growth of the crystal. Therefore, a lower molar concentration of $FeCl_2$ anisotropic (rod-shaped) growth of nanoparticles is observed. As we increase the concentration of $FeCl_2$ isotropic growth, it replaces the directed growth of Fe_3O_4 crystals due to the high concentration of $FeCl_2$. Since nucleation and growth steps are not separate in case of high-concentration samples, these nucleated nanocrystals of Fe_3O_4 tend to form Fe_3O_4 sphere without any specific growth directions, which is thermodynamically favored morphology.

Magnetic Properties of Nano-sized Fe_3O_4

The magnetization vs. magnetic field (M-H) variations of different shaped and sized Fe_3O_4 samples were analyzed by using Physical Properties Measurement System (PPMS) having the facility to vary the magnetic field up to 14 T. Hysteresis loops of various Fe_3O_4 samples have been shown in Fig. 3a, b recorded at 300 and 5 K, respectively. These figures give some useful information about the magnetic response of various samples. All samples show a nonlinear variation in magnetization as a function of magnetic field at both temperatures

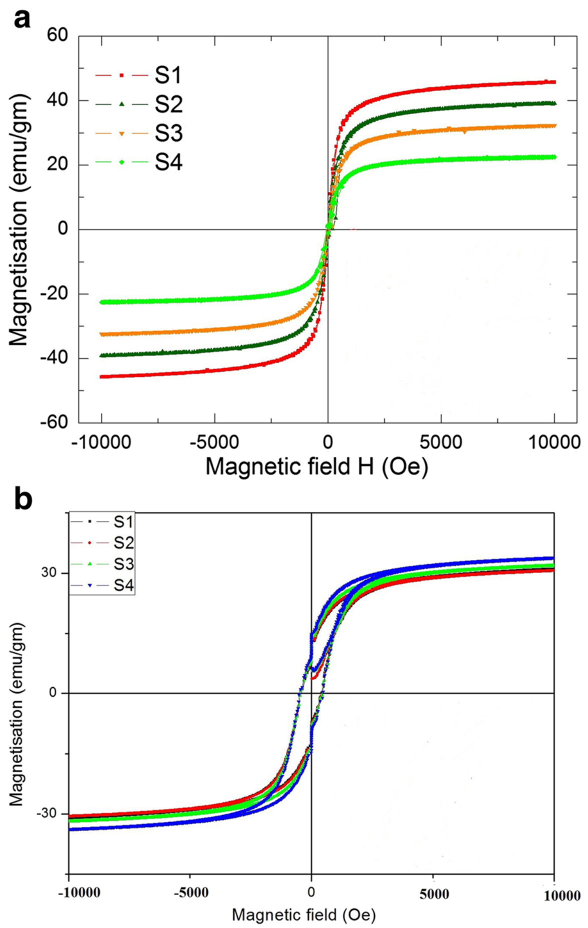

Fig. 3 **a** Magnetization vs. magnetic field plot of different Fe_3O_4 samples at 300 K. **b** Magnetization vs. magnetic field plot of different Fe_3O_4 samples at 5 K

(300 and 5 K). Figure 3a is a typical M-H curve for all four samples at measured at 300 K. It is evident that magnetic remanence is almost absent in all samples. Another peculiar feature is initial slopes in magnetization curves at 300 K of all samples are very steep. These observations can be explained by surface effect and finite size effect. Incorporation of these effects on a magnetic system suggests that particles are small enough to be considered as single-domain particles. These single domains orient as a large single magnetic moment in the direction of applied field. Because of the single-domain nature of particles, it shows almost no remnant magnetization after removal of external applied magnetic field. The values of Mr, Ms, and Hc of all samples are given in the table. Further, Fig. 3b shows the M-H plot of the same samples at 5 K. The behavior of this graph is very different from the M-H plot at 300 K. The distinct feature of this graph is Hc which began to appear with large value with respect to Hc at 300 K. This results in the disappearing superparamagnetic behavior of particles. Further in this case (Fig. 3b), saturation magnetization is almost the same for all samples, but in Fig. 3a, different samples show different saturation magnetization. Figure 4a, b is the plot of Mr, Ms, and Hc as a function of molarity calculated from inset of Fig. 3a, b, at 300 and 5 K, respectively. A careful observation of Fig. 4a indicates that the coercivity (Hc) of the samples have been found to increase monotonously with the decrease in the aspect ratio of the magnetic nanostructures (from 10.60 to 42.30 Oe). The Hc value of the rod-shaped nanostructures having the largest aspect ratio (S_1) is the least and vice versa. It indicates that the magnetization of the elongated particles is more sensitive to the applied field than that of the particles having less aspect ratio [22]. These figures show explicitly the effect of temperature on Mr, Ms, and Hc. A notable change appears in Hc as we cool the samples up to 5 K. Hc monotonously decreases for all samples as we increase the temperature. This behavior can be understood as due to enhancement in thermal energy via temperature will enhance the thermal fluctuations of pinned magnetic moments, therefore, minimizing the effect of anisotropy barriers. This appearance of coercivity at low temperature destroys the superparamagnetic behavior of Fe_3O_4 nanoparticles, which is the characteristic feature of Fe_3O_4

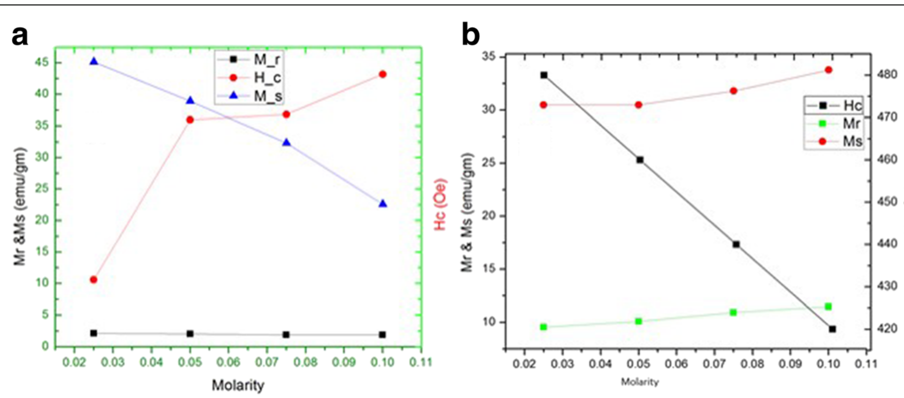

Fig. 4 **a**, **b** Variation of Mr, Ms and Hc as a function of molarity for different samples at 300K and 5K respectivly

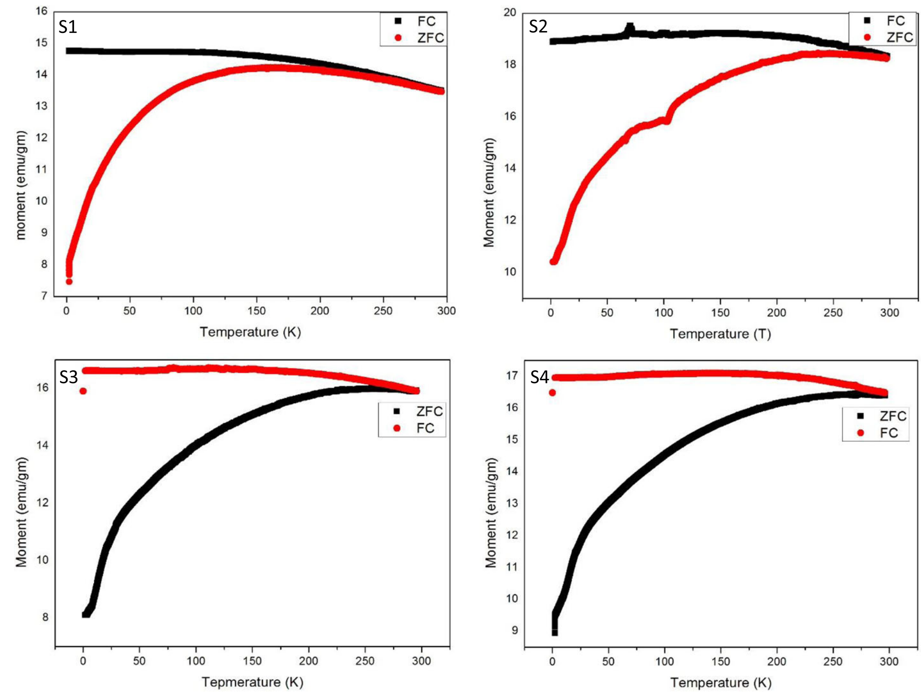

Fig. 5 Magnetisation vs temperature plot of different Fe_3O_4 samples (S1-S4)

nanoparticles at 300 K. Numerical values of Mr, Ms, and Hc have also been incorporated in the table. The data recorded at 300 K are much improved than reported earlier [21].

Further, magnetization vs. temperature (M-T) measurement of as-prepared Fe_3O_4 nanoparticles of different shapes and sized was investigated using PPMS. Zero-field-cooling (ZFC) and field-cooling (FC) processes were used to study the magnetization vs. temperature profile of synthesized nanoparticles between 5 and 300 K at 500 Oe (Fig. 5). FC and ZFC curves are usually utilized to understand the energy barriers [23]. Figure 5 shows the magnetization response as a function of temperature for all four samples (S_1, S_2, S_3, and S_4). All samples were in powder form while undergoing for measurement. When the sample is cooled at very low temperature (~5 K), the net magnetic moment is negligibly small as the magnetic moment of every individual particle is randomly oriented. When the external magnetic field is applied, randomly oriented moments begin to align in the direction of the field. Therefore, net magnetic moment increases gradually and reaches up to a maximum (169, 246, 250, and 266 K for S_1, S_2, S_3, and S_4, respectively). The temperature at which magnetization is maximum is known as blocking temperature (T_B). This is also defined as the temperature at which thermal energy is in equilibrium with the energy of aligned magnetic moments. As the temperature rises greater than the blocking temperature, thermal energy begins to destroy the alignment of moments and hence resulting in a decline of magnetization above T_B. Further, it may be pointed out from graphs that FC and ZFC curves behave in a similar way above blocking temperature which is different for all samples [24, 25].

Some useful parameters of M-T and M-H measurements have been given in Table 1.

Mechanism of Formation of Fe_3O_4 Nanoparticles

Our synthesis protocol initially requires the aqueous solution of $FeCl_2$. Reaction is as follows:

Table 1 Some useful parameters of M-T and M-H measurements

Sample name	Mr (emu/g) at 300 K	Ms (emu/g) at 300 K	Hc (Oe) at 300 K	Mr (emu/g) at 5 K	Ms (emu/g) at 5 K	Hc (Oe) at 5 K	T_B (K)
S_1	2.13	45.15	10.60	9.54	30.49	480	169
S_2	2.01	38.95	36.00	10.17	30.44	465	246
S_3	1.90	32.30	36.85	10.91	31.81	440	250
S_4	1.87	22.60	43.20	11.45	33.78	425	266

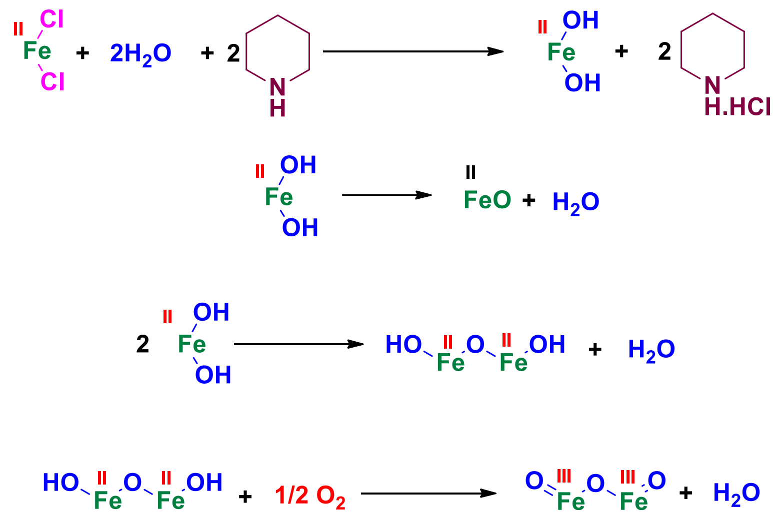

Fig. 6 (1) The first step is the hydrolysis of $FeCl_2$ by water in presence of piperidine which facilitates the hydrolysis by neutralizing HCl produced in the reaction and hence making the reaction move in forward direction. (2) The next step is dehydration of $Fe(OH)_2$ to produce ferrous oxide. (3) The similar dehydration of two molecules of ferrous hydroxide produces $H_2Fe_2O_3$ which on spontaneous aerial oxidation produces the Fe_2O_3. (4) The FeO and Fe_2O_3 combine to give Fe_2O_4

$$FeCl_2 + 2H_2O \rightarrow Fe(OH)_2 + 2HCl$$

This is a reversible reaction with almost equal forward and backward reaction rate. After adding piperidine in the reaction mixture, HCl gets trapped with piperidine, making the reaction in the forward direction only. This leads to the formation of stable $Fe(OH)_2$. This $Fe(OH)_2$ undergoes dehydration process to produce FeO. Similar process occurs with two FeO molecules resulting in the formation of $H_2Fe_2O_3$, which on spontaneous aerial oxidation gives Fe_2O_3. In the final step of the reaction, FeO and Fe_2O_3 get combined to produce Fe_3O_4. This whole process is represented in pictorial form (Fig. 6).

Conclusion

Conclusions of the current study can be summarized as follows:

1. Fe_3O_4 nanoparticles are indeed synthesized using piperidine, which is confirmed by XRD characterization of as-synthesized samples.
2. TEM images give some useful information related to the shape and sizes of the particles. Our investigation shows that shape and size of the particles can be changed from rods to spheres by varying the molar concentration of $FeCl_2$ solutions (from 0.025 to 0.1 M).
3. Measurement of magnetic properties found after deep analysis shows that these magnetic parameters like Ms, Mr, Hc, and T_B have shown improved values than reported earlier.
4. These synthesized Fe_3O_4 nanoparticles of different shapes and sizes will further be used for their applications like EMI shielding. Some primitive experiments are going on and very soon will be followed by respective publications.

Acknowledgements
Authors are thankful to AIRF for the various measurements. AKS is especially thankful to UGC for the DSK PDF and UPE-II which have provided the financial support for the research. Further support from DST-FIST is gratefully acknowledged.

Funding
This study was funded by UPE-II/(172) and UGC/(BSR/14-15/0078).

Authors' Contributions
AKS performed the experiments and characterizations. KS has done the magnetic measurements and its explanetion. ONS has drafted the paper. All authors read and approved the final manuscript.

Competing Interests
The authors declare that they have no competing interests.

Publisher's Note
Springer Nature remains neutral with regard to jurisdictional claims in published maps and institutional affiliations.

Received: 15 February 2017 Accepted: 29 March 2017
Published online: 26 April 2017

References

1. Brust M, Kiely CJ (2002) Some recent advances in nanostructure preparation from gold and silver: a short topical review. Colloids Surf A Physicochem Eng Asp 202:175–186
2. Alivisatos AP (1996) Semiconductor clusters, nanocrystals, and quantum dots. Science 271:933–937
3. Cengelli F, Grzyb JA, Montoro A, Hofmann H, Hanessian S, Juillerat-Jeanneret L (2009) Surface-functionalized ultrasmall superparamagnetic nanoparticles as magnetic delivery vectors for camptothecin. ChemMedChem 4:988–997
4. Chen B, Lai B, Cheng J, Xia G, Gao F, Xu WJ, Gao C, Sun X, Xu C, Chen W, Chen N, Liu L, Li X, Wang X (2009) Daunorubicin-loaded magnetic nanoparticles of Fe_3O_4 overcome multidrug resistance and induce apoptosis of K562-n/VCR cells in vivo. Int J Nanomed 4:201–208

5. Howes P, Green M, Bowers A, Parker D, Varma G, Kallumadil M, Hughes M, Warley A, Brain A, Botnar R (2010) Magnetic conjugated polymer nanoparticles as bimodal imaging agents. J Am Chem Soc 132:9833–9842
6. Li Calzi S, Kent DL, Chang KH, Padgett KR, Afzal A, Chandra SB, Caballero S, English D, Garlington W, Hiscott PS, Sheridan CM, Grant MB, Forder JR (2009) Labeling of stem cells with monocrystalline iron oxide for tracking and localization by magnetic resonance imaging. Microvasc Res 78:132–139
7. Balivada S, Rachakatla RS, Wang H, Samarakoon TN, Dani RK, Pyle M, Kroh FO, Walker B, Leaym X, Koper OB, Tamura M, Chikan V, Bossmann SH, Troyer DL (2010) A/C magnetic hyperthermia of melanoma mediated by iron (0)/ iron oxide core/shell magnetic nanoparticles: a mouse study. BMC Cancer 10:119–127
8. Parekh K, Upadhyay RV, Mehta RV (2005) Magnetic and rheological characterization of Fe_3O_4 ferrofluid. Hyperfine Interact 160:211–217
9. Bautista FM, Campelo JM, Luna D, Marinas JM, Quiros RA, Romero AA (2007) Screening of amorphous metal–phosphate catalysts for the oxidative dehydrogenation of ethylbenzene to styrene. Appl Catal B 70:611–620.
10. Fried T, Shemer G, Markovich G (2001) Ordered two-dimensional arrays of ferrite nanoparticles. Adv Mater 13:1158–1161
11. Zhu J, Wei S, Chen M, Gu H, Rapole SB, Pallavkar S, Ho TC, Hopper J, Guo Z (2013) Magnetic nanocomposites for environmental remediation. Adv Powder Technol 24:459–467
12. Yang T, Wen X, Ren J, Li Y, Wang J, Huo C (2010) Surface structures of Fe 3 O 4 (111), (110), and (001): a density functional theory study. J Fuel Chem Technol 38:121–128
13. Gupta AK, Gupta M (2005) Synthesis and surface engineering of iron oxide nanoparticles for biomedical applications. Biomaterials 26:3995–4021
14. Wanga X, Zhangb Y, Wu Z (2010) Magnetic and optical properties of multiferroic bismuth ferrite nanoparticles by tartaric acid-assisted sol–gel strategy. Mater Lett 64:486–488
15. Dacoata GM, Degrave E, Debakker PMA, Vandenberghe RE (1994) Synthesis and characterization of some iron oxides by sol-gel method. J Solid State Chem 113:405–412
16. Hyeon T, Lee SS, Park J, Chung Y, Na HB (2001) Synthesis of highly crystalline and monodisperse maghemite nanocrystallites without a size-selection process. J Am Chem Soc 123:12798–12801
17. Abu Mukh-Qasem R, Gedanken A (2005) Sonochemical synthesis of stable hydrosol of Fe_3O_4 nanoparticles. J Colloid Interface Sci 284:489–494
18. Wang ZL (2000) Transmission electron microscopy of shape-controlled nanocrystals and their assemblies. J Phys Chem B 104:1153–1175
19. Sun YG, Xia YN (2002) Shape-controlled synthesis of gold and silver nanoparticles. Science 298:2176–2179
20. Xiong Y, Xia Y (2007) Shape-controlled synthesis of metal nanostructures: the case of palladium. Adv Mater 19:3385–3391
21. Sun S, Zeng H, Robinson DB, Raoux S, Rice PM, Wang SX, Li G (2004) Monodisperse MFe_2O_4 (M = Fe, Co, Mn) nanoparticles. J Am Chem Soc 126:273–279
22. He X, Zhong W, Chak-Tong A, Du Y (2013) Size dependence of the magnetic properties of Ni nanoparticles prepared by thermal decomposition method. Nanoscale Res Lett 8:446–450
23. Rondinone AJ, Samia ACS, Zhang ZJJ (1999) Superparamagnetic relaxation and magnetic anisotropy energy distribution in $CoFe_2O_4$ spinel ferrite nanocrystallites. Phys Chem B 103:6876–6880
24. Cao H, Liang R, Qian D, Shao J, Qu M (2011) L-Serine assisted synthesis of superparamagnetic Fe_3O_4 nanocubes for lithuim ion batteries. J Phys Chem C 115:24688–24695
25. Yang T, Shen C, Li Z, Zhang H, Xiao C, Chen S, Xu Z, Shi D, Li J, Gao H (2005) Highly ordered self-assembly with large area of Fe_3O_4 nanoparticles and the magnetic properties. J Phys Chem B 109:23233–23236